*Tellus (1995), 47B, 178–190*
*Printed in Belgium – all rights reserved*


TELLUS
*ISSN 0280–6509*

# Monitoring seasonal and interannual variations of gross primary productivity, net primary productivity and net ecosystem productivity using a diagnostic model and remotely-sensed data

By P. MAISONGRANDE[1]*, A. RUIMY[2], G. DEDIEU[1] and B. SAUGIER[2], [1]*Laboratoire d'Etudes et de Recherches en Télédétection Spatiale, Unité mixte CNES-CNRS, Toulouse, France*; [2]*Laboratoire d'Ecologie Végétale, Université de Paris Sud, CNRS, Orsay, France*

(Manuscript received 2 December 1993; in final form 16 September 1994)

ABSTRACT

A new diagnostic model for the estimation of net primary productivity (NPP) is presented. It is derived from the Kumar and Monteith model for remote sensing of crop growth, with a separate parameterization of autotrophic respiration. The NPP model is coupled to a soil respiration model, calibrated in order to balance the resulting net ecosystem productivity (NEP) over a year. This model is run over the years 1986 to 1991 with NOAA-AVHRR derived normalized difference vegetation index (NDVI) as inputs, for which the radiometric calibration drift has been accounted for. The outputs of the model are analyzed in terms of interannual variations: the model seems to be able to simulate the effects of events such as El Niño on the terrestrial net primary productivity. The NEP outputs are compared to $CO_2$ concentration measurements in the atmosphere, on a zonally averaged basis, without taking into account atmospheric transport. Seasonal evolution of NEP and atmospheric $CO_2$ are well in phase in latitudes of the temperate northern hemisphere, but the correspondence is weaker or absent in the tropics and southern hemisphere.

## 1. Introduction

The terrestrial biosphere acts in the global carbon cycle through the process of net ecosystem productivity (NEP), which is the balance of net primary productivity of the vegetation (NPP), and heterotrophic decomposition or soil respiration (SR). NPP, the rate of carbon uptake by vegetation, is the balance between photosynthetic gross primary productivity or GPP, and autotrophic respiration. These processes are driven by climatic variables such as solar radiation, temperature, precipitation, etc., with response functions that are different for each process. In this paper we present a preliminary version of a diagnostic model of GPP, NPP and NEP.

The model for GPP, NPP and NEP that we use in this analysis is based on a parametric model derived from the Monteith NPP model (1972, 1977), and the Kumar and Monteith (1981) model of remote sensing of crop growth: NPP is the product of incident solar radiation by various efficiencies, the efficiency of solar radiation absorption being related to a satellite-derived vegetation index. It has been first used on a global scale by Heimann and Keeling (1989). Our improvements consist in applying this model to GPP, to which it is more adapted than to NPP, and to compute autotrophic respiration independently. The use of a satellite-derived vegetation index is a good way to take into account phenological development of the leaf area index (LAI), as well as the effects of

* Corresponding author: P. Maisongrande, LERTS, 18 avenue Edouard Belin, 31055 Toulouse Cedex, France.

prolonged water stresses that reduce the LAI. Thus, the most important factors that drive NPP are taken into account by this model.

The availability of NOAA-AVHRR global vegetation index (GVI product, Tarpley et al., 1984) for the years 1986–1991 allowed us to run such a diagnostic model for these years. The interannual variations of estimated NPP fluxes can be related to the effects of interannual climatic changes, such as El Niño events.

In a first step, we expect that this linkage of different simple components of terrestrial biosphere will give us the mean trends of global NEP fluxes. Then, a possible improvement and validation of such a model on a global scale is to introduce the net fluxes of $CO_2$ to and from the terrestrial biosphere and their isotopic composition in a general circulation model (GCM), along with the fluxes due to the other components of the global carbon cycle (oceanic fluxes, fossil fuel emissions, etc.), and to compare predicted $CO_2$ and carbon isotope concentrations in the atmosphere with local measurements. A simpler, preliminary study is presented in this article, where computed NEP is merely compared with measurements of $CO_2$ concentrations in the atmosphere. The qualitative comparisons give us indications about the ability of the model to simulate some of the spatial, seasonal and interannual variations of NEP fluxes, at least in the cases where $CO_2$ concentrations in the atmosphere are primarily driven by NEP fluxes, when atmospheric transport and other carbon fluxes have low effects comparatively.

Validation of a diagnostic NEP model applied to several years is an important issue in the frame of global carbon cycle studies, particularly because it could help us in the future to calibrate or validate prognostic, physiology-based models that are the only ones able to predict the impact of climate change on vegetation (Kergoat et al., 1995).

## 2. Materials and methods

### 2.1. Model description

*2.1.1. Net primary productivity (NPP).* The NPP model we use is derived from Monteith (1972, 1977), which considers NPP as the product of solar energy by various yields, or efficiencies of conversion. In the original model for crop growth remote sensing (Kumar and Monteith, 1981), NPP is the product of 3 efficiencies by the incident global radiation:

$$\mathrm{NPP}(t) = ef(t)\, cS_0(t), \tag{1}$$

with $t$: time; $c$: "climatic efficiency", i.e., the ratio between incident photosynthetically active radiation (PAR) and incident global radiation $S_0$; in this study, it is fixed to 0.48 (McCree, 1972); $f$: "absorption efficiency", i.e., the ratio (PAR absorbed by the canopy)/(incident PAR); $e$: "conversion efficiency", i.e., the ratio (dry matter produced)/(absorbed PAR). $f$ is assumed to be linearly related to the remotely sensed normalized difference vegetation index or NDVI (Asrar et al., 1984):

$$f(t) = A + B\,\mathrm{NDVI}(t). \tag{2}$$

$A$ and $B$ were calibrated using minimum and maximum NDVI values for the 6 years of the study, in order to obtain an intercept equal to zero for deserts and a maximum intercept for equatorial forest ($0 \leqslant f(t) \leqslant 1$). The main error in using a linear relationship between $f$ and NDVI, is expected in areas with low LAI (LAI $< 3$). In this case, soil reflectance acts as a background signal influencing NDVI: for a given vegetation development, NDVI decreases as soil-brightness increases (see Huete, 1989, for a detailed discussion). Errors induced by this problem amount to about 10%. Surface directional effects may also influence the signal through a significant increase or decrease of reflectances. Nevertheless, these effects are averaged and then minimized when considering annual GPP.

This model has been used on a global scale by Heimann and Keeling (1989) with a constant $e$ of about 2.8 g dry matter produced per MJ of PAR absorbed, corresponding to a mean of $e$ values for crops in Great Britain (Monteith, 1977). As $e$ actually varies with several environmental and vegetation-related parameters, a previous study has been made using biome-dependant values of $e$ (Ruimy et al., 1994). However, the lack of values of $e$ for some vegetation types and environmental conditions leads us to try to model the variations of $e$ with these parameters. The literature compilation of $e$ values for different biomes (Ruimy et al., 1993) shows that $e$ decreases from boreal to



Tellus B/47/1/2-13

equatorial vegetation types (globally correlated with temperature, one determinant of respiration), and is greater for grasslands than forests (globally correlated with biomass, another determinant of respiration). We assume that this dependance of $e$ on temperature and biomass is due to autotrophic respiration, while the photosynthetic efficiency, $e'$, should be more conservative. We have therefore the following model:

$$\begin{aligned}\mathrm{NPP}(t) &= [1 - r(t)]\ \mathrm{GPP}(t) \\ &= [1 - r(t)]\ e' f(t)\ cS_0(t),\end{aligned} \tag{3}$$

with $e'$: "photosynthetic efficiency", i.e., the ratio (assimilates produced by net assimilation)/(absorbed PAR); $r$: "respiratory losses": fraction of assimilates photosynthetized lost by autotrophic respiration.

In this study, the parameterization of $e'$ was done by plotting daily $CO_2$ fluxes measured above canopies against absorbed PAR for several vegetation types. Ruimy et al. (personal communication) did a compilation of literature on $CO_2$ flux measurements over plant canopies, in relation to intercepted solar radiation. The result is that if we plot daily integrated $CO_2$ flux versus solar radiation for all the available data sets, the best fit through this data set is linear. The slope of the linear regression is taken to be $e'$, the "photosynthetic efficiency" ($e' = 4.45$ g $CO_2$ assimilated per MJ of PAR absorbed). Respiration can be decomposed into maintenance respiration, depending on plant biomass and temperature, and growth respiration, proportional to net assimilation (McCree, 1974). Global data sets on biomass exist (Olson et al., 1983), but it is not easy to use this information in a consistent way with our satellite based GPP model. In this preliminary study, we use a simplified model where $r$, the respiratory losses, depend on temperature only: the parameterization of Goward and Dye (1987):

$$r(t) = \frac{(7.825 + 1.145T(t))}{100}, \tag{4}$$

with $T$: temperature (°C).

This empirically-derived equation is used by Goward and Dye (1987) to calculate autotrophic respiration on the North American continent which also include tropical zones. As North America includes most types of the world terrestrial ecosystems, we applied eq. (4) at the global scale. Although leaf respiration can be considered proportional to leaf biomass, NDVI saturation at LAI greater than about 3 probably leads to an underestimation of $r(t)$ at high LAI (but not of $f(t)$). As respiration is derived from GPP, it also induces an underestimation during the leafless period when roots and woody organs still respire. This effect has high sensitivity in regions of warm temperature in leafless period, but low effects on cold deciduous ecosystems. We are currently working on independent models of autotrophic respiration function of biomass and temperature.

*2.1.2. Soil respiration (SR).* Although the $CO_2$ flux from the soil to the atmosphere depends on several environmental and soil-related parameters (biome, carbon content of the soil, humidity, ...), temperature is known to be the dominant factor determining heterotrophic respiration fluxes. In this study, we use an exponential dependency on this parameter:

$$\mathrm{SR} = KQ_{10}^{T/10}, \tag{5}$$

with $K$: heterotrophic respiration coefficient; $Q_{10}$: relative increase of respiration flux for a 10° increase in temperature $T$ ($Q_{10} = 1.5$ in this study).

In this preliminary study, in order to parameterize the coefficient $K$, we have considered the biosphere in equilibrium over a year on each pixel (approach of Heimann and Keeling (1989) for instance):

$$K = \frac{\sum_t \mathrm{NPP}(t)}{\sum_t Q_{10}^{T(t)/10}}. \tag{6}$$

A $K$ coefficient is calculated this way for each pixel and each year. We set $Q_{10} = 1.5$ instead of the values observed in field experiments, which usually range from 2 to 3. Indeed, we modelled SR as a function of air temperature which has stronger annual variations than soil temperature usually used to determine $Q_{10}$. Being aware of the weaknesses of this model (especially at low temperatures where it underestimates fluxes), we assume that this formulation is able to simulate the main trend of SR at the global scale. Our approach should be improved in the future by using another modelling, accounting for litter decomposition and a soil compartment with a longer turnover. This

way, the pattern of heterotrophic respiration should be closer to a comprehensive description of involved phenomena, and should allow to estimate SR independently of NPP over short time scales.

### 2.2. *Input data sets*

*2.2.1. Time and space resolution.* For this study, all input data sets have been interpolated to the weekly time resolution of the remotely sensed data we used. All sets have been registered to Plate Carrée projection, with a $1° \times 1°$ resolution, from 75° N to 55° S, and 180° W to 180° E.

*2.2.2. NDVI.* Normalized Difference Vegetation Index is a combination of reflectances in the visible, $\rho_1$, and near infrared, $\rho_2$, domains of the solar spectrum:

$$\mathrm{NDVI} = \frac{\rho_2 - \rho_1}{\rho_2 + \rho_1}. \tag{7}$$

In this study, we used the second generation of NOAA/AVHRR GVI product (Tarpley et al., 1984) from 1986 to 1991 (NOAA 9 from 1 January 1986 to 7 November 1988, NOAA 11 from 8 November 1988 to 31 December 1991). This product provides raw digital counts in visible and near infrared spectral bands on a weekly basis, as a result of a cloud screening technique based on the maximum NDVI of the week (Holben, 1986). Using the temporal drift of sensor calibrations estimated by Kaufman and Holben (1993), we first computed top of the atmosphere reflectances in both channel, at the GVI resolution. NDVI is then derived after averaging the reflectances at the $1° \times 1°$ resolution. The calibration is based on temporal interpolation of 13 gain coefficients from April 1985 to December 1992. This results in calculated "top of atmosphere" NDVI (TOA NDVI), which are much less variable interannually than the raw NDVI because calibration coefficients have variations up to 15% for each channel, NOAA 9 leading to the most variable reflectances.

Cloud contamination remains a problem, especially over equatorial forest where the probability to obtain a clear scene per week is very low. Therefore, a more drastic cloud screening will be applied in a future experiment in order to stick closer to the real envelope of NDVI.

*2.2.3. Temperature.* Temperature is extracted from the Leemans and Cramer (1991) database, which gives monthly mean temperatures for 30 years. The grid values were resampled from the $0.5° \times 0.5°$ resolution to $1° \times 1°$, and linearly interpolated at the weekly time step. In the future, interannual variability of temperatures could be taken into account using monthly surface air temperature anomalies available from 1880 until December 1990 from weather stations (GISS monthly deviations for equal square boxes, greenhouse effect detection experiment database, Hansen and Lebedeff, 1987; Spangler and Jenne, 1990).

*2.2.4. Solar radiation.* Incoming global solar radiation at the surface is derived on a monthly basis from an output of GCM of the French Meteorological Office (Planton et al., 1991). The original Gauss projection with a latitude-dependent resolution of about 2.8° has been converted to a regular 1°x1° resolution, and linearly interpolated to a weekly time step. The approach will be soon greatly improved by using remote sensing-derived solar radiation fields. Satellite based global solar radiation maps are currently being processed by NASA Langley Research Center for WCRP/GEWEX (Whitlock et al., 1993; Di Pasquale and Whitlock, 1993).

*2.2.5. Atmospheric $CO_2$ measurements.* The measurements of $CO_2$ concentration in the atmosphere are taken from the carbon dioxide Information Analysis Center (CDIAC) database (Conway and Tans, 1990). We have kept only the measurements from the stations where the $CO_2$ was sampled for all the years of our study: 1986–1991. The monthly values of $CO_2$ concentrations for the resulting 20 stations were linearly interpolated to a weekly time step.

## 3. Results and discussion

We have run our model from 1986 to 1991, using the NOAA-AVHRR derived TOA NDVI for these years, but we used monthly climatologies for all the weather data: radiation and temperature. For our preliminary study, we considered that interannual variations in solar radiation and temperature are small compared to changes in remotely sensed vegetation indices, which

integrate well the effects of changes in rainfall. Indeed, the use of NDVI to estimate absorption efficiency allows one to take into account some of the soil moisture effects. For example, long term drought effects are primarily to reduce the LAI and therefore the absorption efficiency, while short terms effects are to reduce stomatal conductance (and then can not be accounted for).

In order to analyze interannual variations of GPP, NPP and NEP, we tried to distinguish between variations connected to the satellite signal (possible uncertainties in the correction of calibration changes, orbital drift of the satellite, changes in atmospheric composition after the Pinatubo eruption), and variations connected to continental-scale climatic changes (the 1986–1987 El Niño event is taken as an example).

### *3.1. $CO_2$ fluxes computed by the model*

*3.1.1. Integrated fluxes for the biosphere.* Table 1 represents the annual NPP for the terrestrial biosphere as computed by our model. Computed GPP is of order 100 Gt of carbon per year, of which 30% is lost in autotrophic respiration. These results are different from commonly admitted values, where GPP would be of the order of 120 Gt($C$), of which 50% would be lost in autotrophic respiration. This indicates that the parameterization of both NPP and respiration should be improved, for example by using a model of the McCree's type for growth and maintenance respiration (McCree, 1974). The underestimation of GPP may be partly due to the method used to derive the solar radiation absorption efficiency ($f$) from NDVI. While other studies, based on one year of NDVI data (Heimann and Keeling, 1989; Ruimy et al., 1994) use the maximum and minimum NDVI value of the considered year to calculate the coefficients $A$ and $B$ (eq. (2)), this study uses the minimum and maximum NDVI of the 6 years from 1986 to 1991. Then, the values of recorded NDVI vary from year to year because of satellite measurements temporal drift (in particular due to orbital drift) and of interannual global climate differences as stressed in this paper. Therefore, the range between the minimum and maximum NDVI of the six years is higher than the one that would be encountered for one year of data. One solution would be to use a set of coefficient for each year.

The global trends of interannual variations are difficult to interpret, because of the small number of years studied. There was an El Niño event in 1986–1987, but in the years 1986 to 1988, the sensor NOAA-AVHRR was recording data of decreasing quality, due to drifting orbit. This orbital drift induced increased solar zenith angles, resulting in larger optical path, decreasing signal, and different directional effects. Years 1989 and 1990 are "good years", satellite-wise, and no special climatic event occurred during these years. Year 1991 saw two superimposing events, the start of an El Niño episode in early 1991, and the eruption of mount Pinatubo in June, which are thought to have opposite effects on the uptake of $CO_2$ by terrestrial ecosystems: El Niño may reduce the global GPP by a reduction in rainfall on some tropical zones, while Pinatubo aerosols may decrease heterotrophic respiration by a decrease of temperatures (Sarmiento, 1993). In addition, Pinatubo aerosols disturb satellite measurements: this issue is discussed in Subsection 3.1.4.

Table 1. *Annual GPP and NPP of the terrestrial biosphere, as computed by our model (unit: $10^{15}$ g of carbon)*

| Year | 1986 | 1987 | 1988 | 1989 | 1990 | 1991 |
|---|---|---|---|---|---|---|
| GPP | 99.1 | 93.1 | 94.8 | 107.9 | 108.2 | 96.7 |
| NPP | 69.2 | 64.8 | 66.5 | 75.3 | 75.6 | 67.7 |
| Satellite | | NOAA-9 | | | NOAA-11 | |
| observation | | 1986–1987 El Niño | NOAA orbital drift | | | 1991–1992 El Niño, Pinatubo |

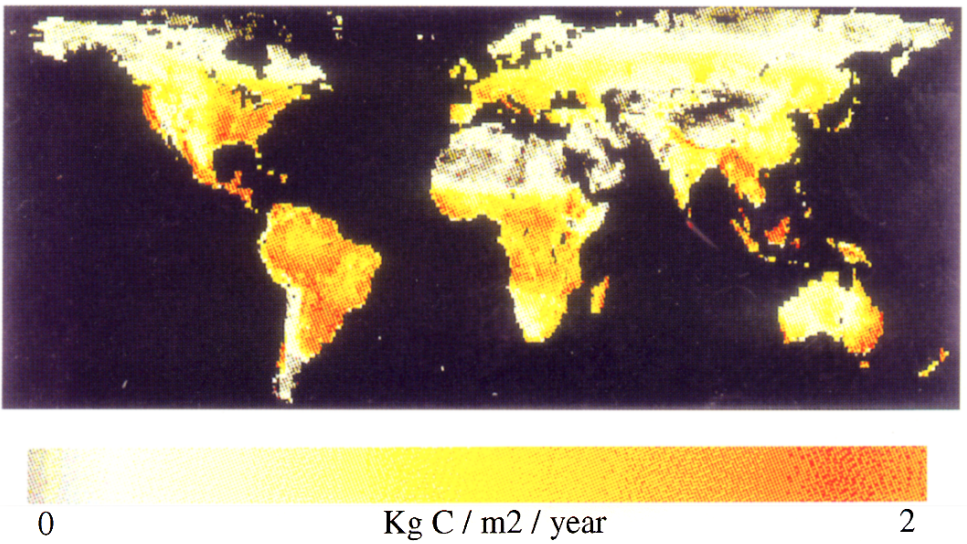


*Fig. 1.* NPP of the terrestrial biosphere in 1989 estimated by our diagnostic model. NPP is integrated over the year, the map is in Plate Carrée projection with a $1° \times 1°$ resolution.

Our ability to analyse interannual variation of NPP strongly depends on the accuracy of NDVI. When the model is run by increasing by 1% TOA NDVI, the annual NPP of the globe is increased by 1.4% (roughly 1 Gt($C$)). This means that, at this stage, the analysis of regional variations is probably more reliable than the discussion of global average evolutions.

*3.1.2. NPP map.* Fig. 1 represents the NPP map computed by our model for 1989 where satellite measurements seem the most reliable. The pattern of NPP distributions is roughly similar to maps obtained by other NPP models such as the Miami model (Lieth, 1975). The main differences are that, in our case, NPP is lower for the Amazonian and African rainforests than for the zones of savannah at the peripheries, while rainforests are the most productive zones in the Miami model, for instance. These differences in NPP estimates for rainforests can be seen also by using the Kumar and Monteith (1981) approach, where eq. (1) is used with $e$ constant all over the world (Ruimy et al., 1994), but it is accentuated by the modulation of $e$ by the autotrophic respiration factor $r$.

*3.1.3. Example study: 1987 El Niño.* Fig. 2 maps differences between the annual NPP for years 1989 and 1987. Differences may be larger than 10%, and are mainly located in south-east Australia, Indonesia, East Africa (Ethiopia/Sudan), southern Africa (Namibia/Botswana/Mozambique), northern parts of Argentina, Bolivia, Central America, and north-west of the US. The year 1987 corresponds to the development of an El Niño event which started late 1986, reached its maximum in mid-1987 and finished in early 1988. This warm ENSO episode was followed by a cold one which lasted until early 1989 (Janowiak and Arkin, 1991). Further analysis is required to establish a possible link between change in NPP and climatic change, particularly precipitation anomalies, induced by El Niño. However, the regional characteristics and amplitude of NPP differences, and the nearly stable NPP in some other large areas can be hardly explained by the already mentioned issues regarding satellite data quality. Calibration drift or changing time of satellite overpasses are mainly acting in the same way over the whole of the Earth.

*3.1.4. Latitudinal, seasonal and interannual variations of zonally averaged fluxes.* Fig. 3

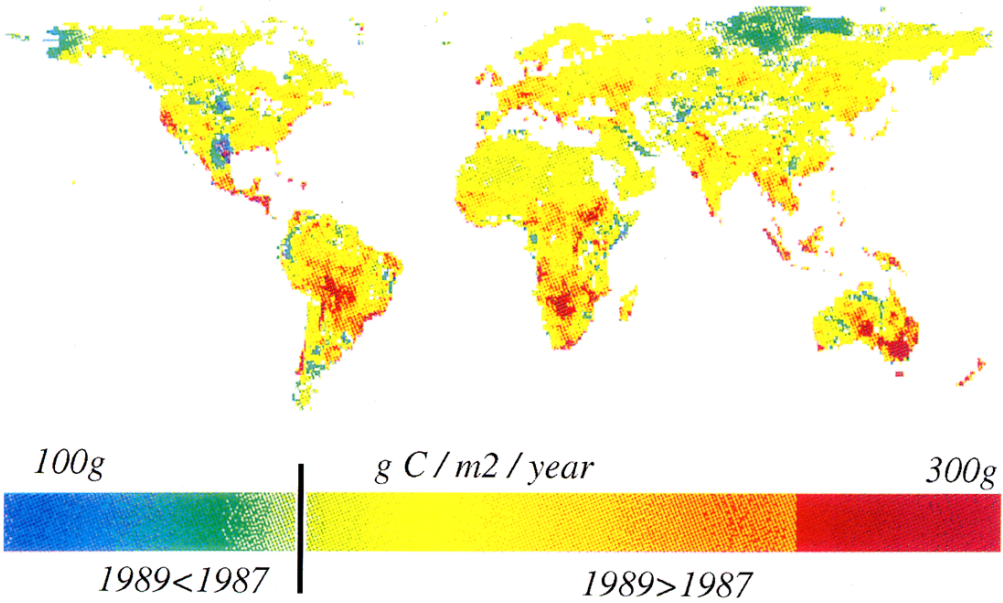


*Fig. 2.* Differences (1989 minus 1987) between the annual NPP of years 1989 and 1987 (El Niño). NPP is integrated over a year, the map is in Plate Carrée projection with a $1° \times 1°$ resolution.

presents annual NPP for 1989 and 1991 as a function of latitude. NPP is cumulated over 1° zonal band. NPP in 1989 and 1991 are rather similar in the northern hemisphere, but NPP estimate in 1991 is smaller than in 1989 for all latitude south of 30° N. A possible explanation for this discrepancy is the effect of the Pinatubo aerosols on the TOA NDVI signal (Stowe et al., 1991). In June 1991, Pinatubo eruption injected a large amount of aerosols in the stratosphere, particularly in the intertropical zone. The most direct effect of this larger optical depth of the atmosphere is a decrease of TOA NDVI for the corresponding area, while we do not expect rapid effects on the vegetation growth and/or the climate conditions in the few months following the eruption.

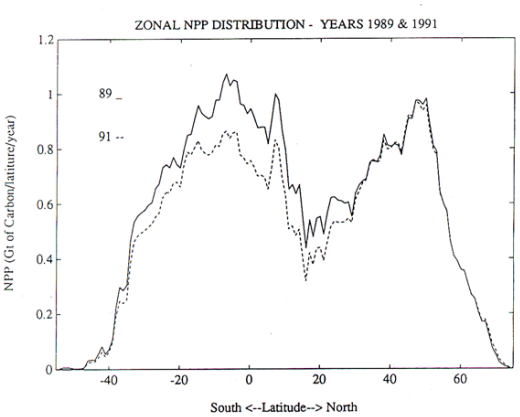


*Fig. 3.* Annual NPP for 1989 and 1991 as a function of latitude. NPP is cumulated over 1° zonal band.

Fig. 4 represents time evolution of weekly, zonally cumulated NPP estimates, from January 1986 to December 1991, for 1° zonal bands and weekly time-step. For each year, the following patterns are observed, as we go from north to south.

- In the temperate northern latitudes, a peak of NPP in the summer, with the length of the growing season increasing as we go towards lower latitudes. This corresponds to cold-deciduous ecosystems.
- In the subtropical northern latitudes, a small peak of NPP in winter, in opposition of phase (maximum in December) corresponding to monsoon-driven ecosystems in eastern orient.
- In the inter-tropical zone, a peak of NPP with a weaker seasonality, roughly in phase with the temperate northern hemisphere peak, corresponding to rainforests and savannahs.

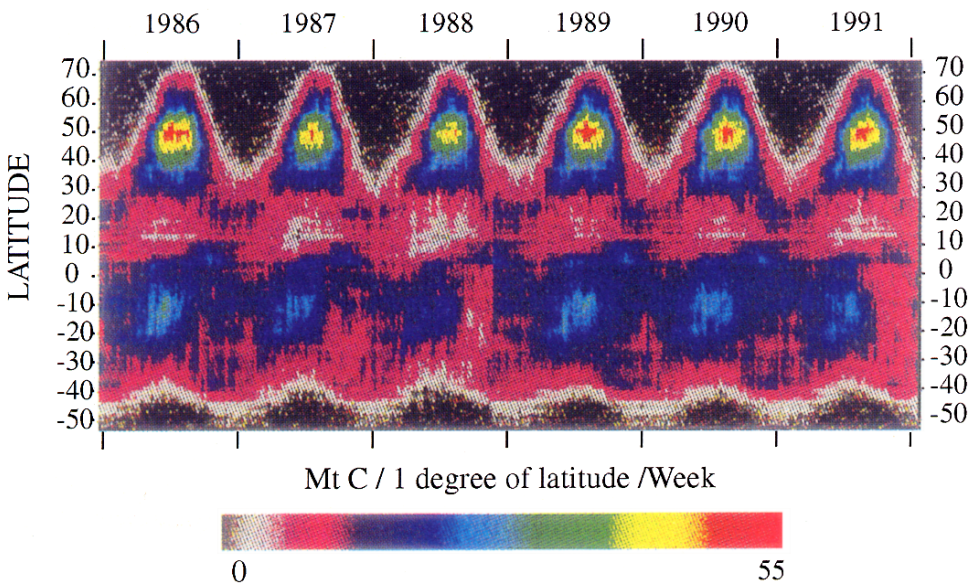


*Fig. 4.* Time evolution of weekly, zonally averaged NPP estimates for the period January 1986 through December 1991, for each 1° zonal band, from 75° N to 55° S (scale units: $10^{12}$ g of carbon).

• In the subtropical/temperate southern hemisphere, south of 25° S, a peak of NPP more localized in space and time than in the northern hemisphere, roughly in opposition of phase with it.

Interannual variations of these patterns reproduce qualitatively the observations of Table 1.

• Year 1988 has a much lower apparent NPP, especially at the level of the equatorial peak. This is attributed to orbital drift of the satellite during this year. Also visible in Fig. 4 is the change from NOAA-9 to NOAA-11 by early November 1988, which leads to change in the time of observations and therefore to different conditions of measurements. In addition, radiometric calibrations change rapidly during the few months following the launch and gain drift corrections are probably less accurate during this period.

• Years 1987 and the beginning of 1991 seem to have lower NPP at the level of the equatorial peak than years 1989 and 1990: this could indicate that the effects of the El Niño years are observable with our GPP model, through the variations of NDVI (the only input with interannual variations). However, to draw conclusions on the observability of the phenomenon with our diagnostic model, we should also account for interannual variations of all the others inputs: radiation and temperature.

• Year 1991 exhibits a sudden decrease of the apparent NPP starting from the middle of the year. As discussed above, this is probably due to the effects of Pinatubo aerosols on the TOA NDVI signal (Stowe et al., 1991).

Fig. 5 represents time evolution of cumulated, zonally averaged NEP estimates, from January 1986 to December 1991, for 1° zonal bands and weekly time-step. When this cumulated NEP is positive (values from yellow to red in Fig. 5), the terrestrial biosphere acts as a sink for atmospheric carbon, while negative cumulated NEP (values from green to violet in Fig. 5) corresponds to a release of carbon to the atmosphere. For each year, we can observe, for each hemisphere, several zones with opposite seasonal cycles. This diagram reads this way: if the peak of NPP occurs in the summer, the cumulated NEP is negative in the first half of the year and positive after; the differences in amplitude reflect the strength of the seasonality: a zone with a marked growing season and a dormant season has two peaks of high amplitude,

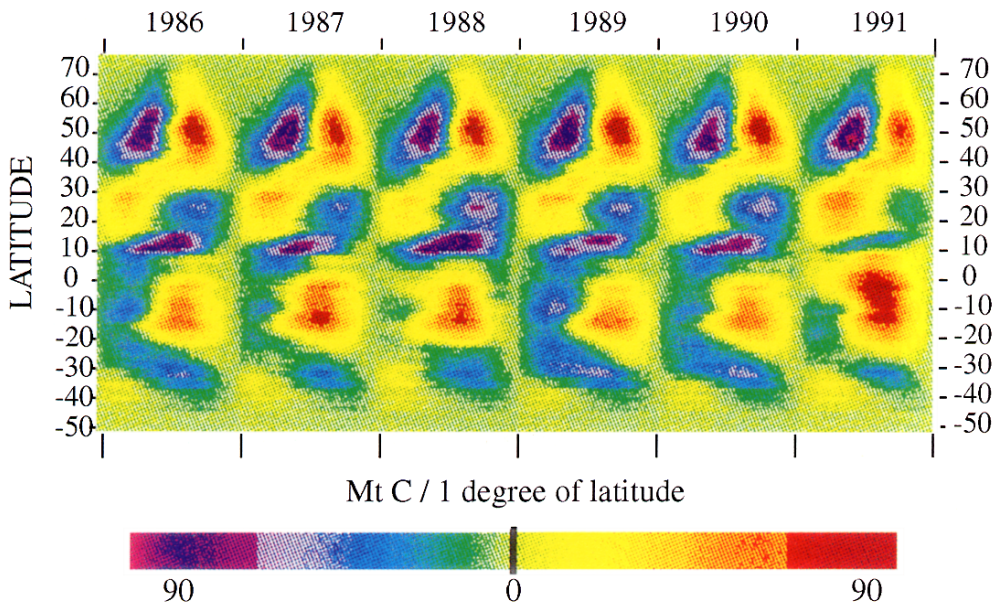


*Fig. 5.* Time evolution of cumulated, zonally averaged NEP estimates for the period January 1986 through December 1991, for each 1° zonal band, from 75° N to 55° S. NEP is cumulated from January 1st to December 31st of each year (scale units: $10^{12}$ g of carbon).

while a zone with sempervirent vegetation has small peaks to no peak at all. In the northern hemisphere, as we go southward, we notice three zones with opposite phases: the boreal/temperate with a growing season peak in summer (cold deciduous), the subtropics (monsoon in Asia) with a peak in winter, the tropics (savannahs of Africa, South America) with a low-amplitude peak in autumn. At the equator there is almost no seasonality. In the southern hemisphere, we notice 2 zones with opposite phases: the tropics (savannahs of Africa, South America) with a peak in spring, the subtropics/temperate zones (South America) with a peak in winter.

### 3.2. *Comparison with atmospheric $CO_2$ composition*

Even though the terrestrial biosphere is not the only compartment exchanging carbon with the atmosphere, and even though mixing occurs in the atmosphere, we can assume that the first phenomenon driving the seasonal variations of $CO_2$ in the atmosphere as measured in $CO_2$ sampling stations is the terrestrial NEP, at least for the northern hemisphere (Heimann et al., 1989). We can therefore use the approach of Tucker et al. (1986) to relate directly fluxes of carbon to and from the terrestrial biosphere to atmospheric $CO_2$ measurements. The improvements we have achieved compared to the work of Tucker et al. (1986) consist in the use of a diagnostic model of NEP with satellite-derived vegetation indices as inputs, instead of directly relating satellite-derived vegetation indices to atmospheric $CO_2$ measurements. This allows us to quantitatively compare time-integrated NEP fluxes computed with calibrated NDVI, and atmospheric $CO_2$ concentrations ($[CO_2]$). On Fig. 6a, NEP levels range from grey to white for positive NEP, while levels from grey to black correspond to negative NEP.

For a sample of 20 measuring stations, we plot (Fig. 6b) the temporal evolution of $[CO_2]$ as a function of time, assuming that each station is representative of the 1° belt where it is located. Grey levels range from black to white for increasing $[CO_2]$. The analysis of the resulting time-latitude diagram shows that from 71.30° N to 40.68° S, the seasonal amplitude is decreasing from north to south, with no obvious seasonal cycle south of 5° S. Few changes in the phasing

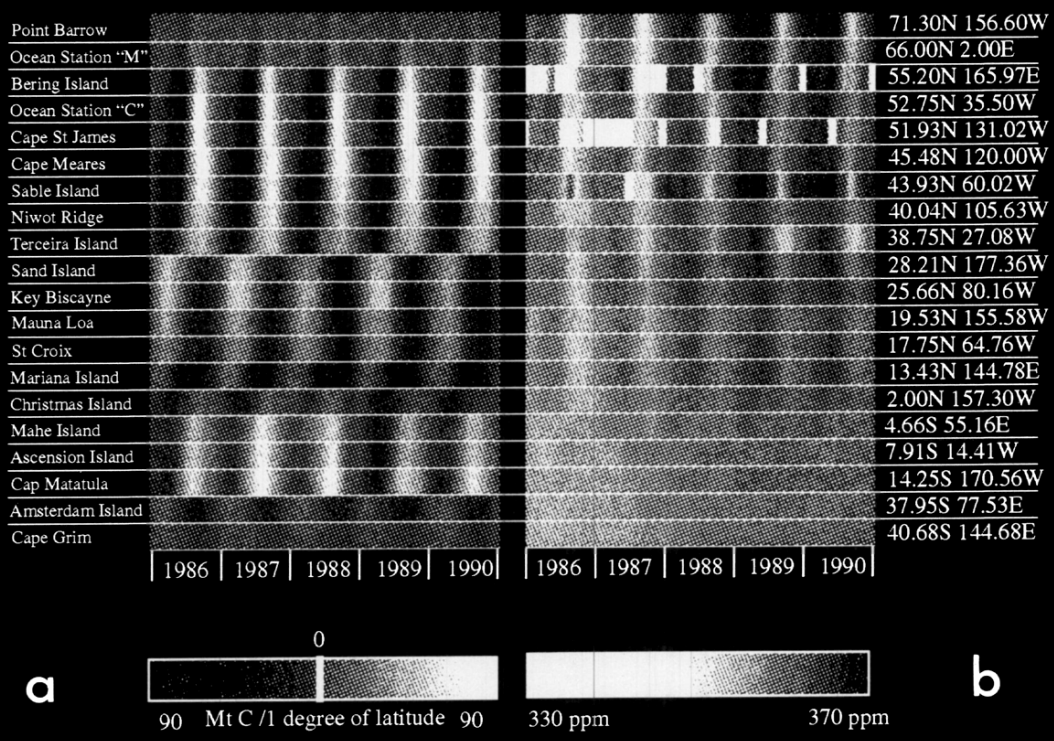


*Fig. 6.* Comparison of temporal evolution of cumulated, zonally averaged NEP estimates (left figure) with variations of $CO_2$ concentrations in the atmosphere (right figure). Left: NEP as in Fig. 5, but for zonal band where atmospheric $CO_2$ concentration measurements were available. Right: temporal evolution of monthly averaged $CO_2$ concentration in the atmosphere, from ground stations (missing data are in black).

of seasonal cycle occur when moving along meridians. As we could expect, Fig. 6b also shows the increasing trend of atmospheric $CO_2$ from 1986 to 1991 whichever the considered station.

Figs. 6a, b allow one to compare qualitatively space and time evolution of cumulated NEP and $[CO_2]$, reminding that positive NEP correspond to a carbon uptake by vegetation and should lead to a decrease of $[CO_2]$. Fig. 6a represents an extraction of the Fig. 5 for the zonal bands presented in Fig. 6b. Contrary to $[CO_2]$, cumulated NEP exhibits well marked seasonal cycle in both hemisphere but with different phases when moving along meridians. As expected if we only consider the role of terrestrial biosphere, $[CO_2]$ and NEP are out of phase of about 6 months in the northern hemisphere, which suggest that NEP is the primary driver of $[CO_2]$ in that region, vegetation removing $CO_2$ from the atmosphere in spring and summer. Between 38° N and 13° N, the main vegetated areas are located in South Asia and Central America, and the observed seasonality is mainly driven by NDVI observations. In this zonal band, the seasonality of NEP is reversed compared to higher latitudes and becomes in phase with $[CO_2]$: this means that some factors are not taken into account in a simple and qualitative interpretation based only on vegetation carbon uptake, and that atmospheric transport and oceanic and anthropogenic sources and sinks must be included in the analysis.

In order to illustrate this general behaviour, we plotted temporal evolution of $[CO_2]$ together with the evolution of cumulated NEP for 1° zonal bands (Fig. 7). For Niwot Ridge (40.4° N, 105.6° E, Fig. 7a) $[CO_2]$ and cumulated NEP are out of phase of 6 months: this can be probably explained by the predominant role of vegetation in driving $[CO_2]$ at this latitude, which includes large proportion of land, and by the location of Niwot

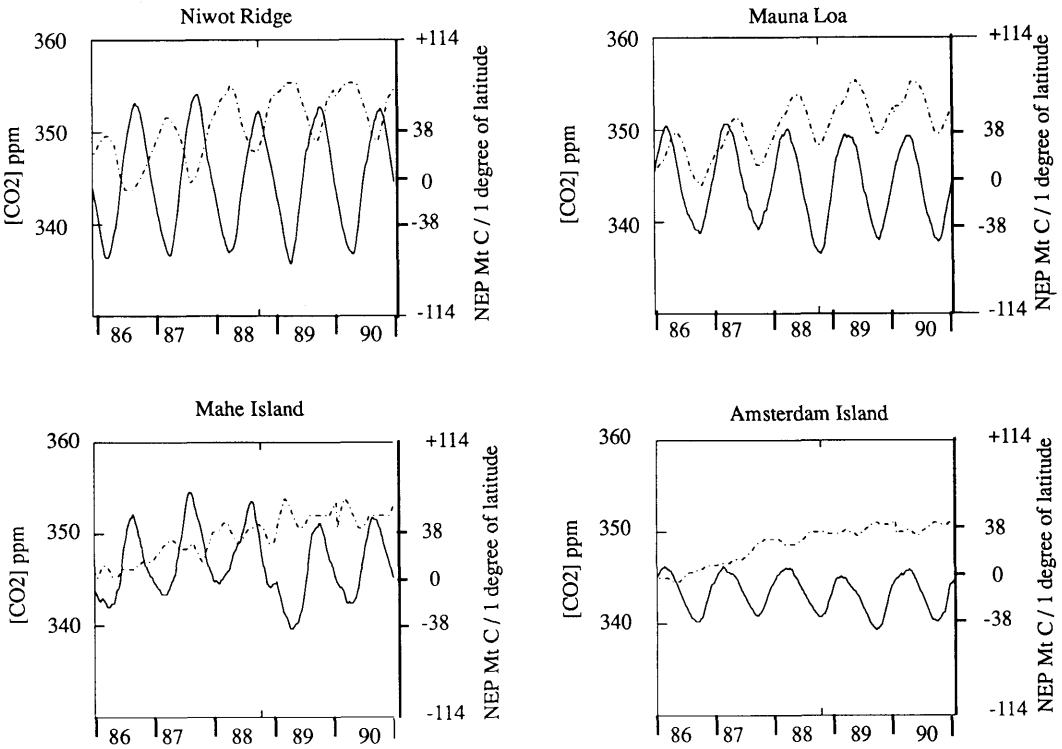


*Fig. 7.* Comparison of temporal evolution of monthly averaged $CO_2$ concentrations in the atmosphere (dotted lines), measured in four different stations, and cumulated NEP fluxes averaged over the corresponding latitude (full lines). The stations are: (a) Niwot Ridge (40.04° N, 105.63° W, (b) Mauna Loa (19.53° N, 155.58° W), (c) Mahé Island (4.66° S, 55.16° E), (d) Amsterdam Island (37.95° S, 77.53° E).

Ridge station in the central US. In a similar plot for Mauna Loa (19.5° N, 155.6° S, Fig. 7b) [$CO_2$] and cumulated NEP are nearly in phase: this station is located in a zonal band with large ocean surface, where, apart from South Asia and Central America, most of the land surface is arid. Finally similar plots for two stations in the southern hemisphere (Fig. 7c, d) show that despite a seasonal cycle in cumulated NEP, atmospheric [$CO_2$] records exhibit weak or even no seasonal cycle.

## 4. Conclusion

The diagnostic model for net primary productivity (NPP) and net ecosystem productivity (NEP) presented here is a potentially interesting model for the study of the role of the terrestrial biosphere in the global carbon cycle. It uses the high spatial and temporal resolution of a remotely sensed vegetation index to simulate NPP on a weekly basis for the years 1986 to 1991. Its inputs are climatic averages of solar radiation and temperature: theses data sets need to be improved to account for the interannual variability. The other two major improvements to be done are: first to parameterize soil respiration independently from NPP (in this version a net flux of zero is assumed over a year on each point), and second: to use an independent model of autotrophic respiration, function of biomass and temperature. In this preliminary study, the model seems to be able to simulate the effects of interannual climate changes such as the 1987 El Niño on regional NPP. The comparison of NEP with measurements of atmospheric $CO_2$ appeared difficult without using an atmospheric transport model. Strong correlations are found only in the northern temperate

latitudes. The seasonal variations of atmospheric $CO_2$ in the whole northern hemisphere seem to be very influenced by northern land masses.

The model used in this study heavily relies on the quality of remotely sensed data. Of particular importance for interannual monitoring of NPP are the corrections for the temporal drift of sensor calibrations and for atmospheric effects, especially when anomalies such as Mt. Pinatubo aerosols occur. Although we attempted to take into account calibration drift for the 1986–1991 period, it is obvious that an improved calibration monitoring is needed because of the large sensitivity of the model to that factor. Mt. Pinatubo aerosols and other atmospheric effects will be corrected in future work. Once these improvements are performed, the atmospheric transport model, with input fluxes from the various carbon reservoirs, and $[CO_2]$ and carbon isotopes measurements, could be used to validate NEP estimates.

The main interest of monitoring temporal and spatial variability of NPP is to identify areas where large changes occur, use these changes to better understand the underlying processes and check the ability of mechanistic models to simulate these changes. As long-term observations are needed for such an exercise, the diagnostic approach described in this paper would benefit of a possible better availability of NOAA/AVHRR archive since the early 80's.

## 5. Acknowledgements

This work is a contribution to the ESCOBA project "The global carbon cycle and its perturbation by man and climate II. Part B: terrestrial biosphere", supported by the Environment Program of the Commission of the European Communities. The authors would like to thank also the "Région Midi-Pyrénées" for funding part of the facilities used to establish the data set archive. P. Maisongrande and A. Ruimy are supported by CNES and MESR through grants. The authors are also indebted to Stéphane Adam for his efficient technical support throughout this study.

## REFERENCES

Asrar, G., Fuchs, M., Kanemasu, E. T. and Hatfield, J. L. 1984. Estimating absorbed photosynthetically active radiation and leaf area index from spectral reflectance in wheat. *Agronomy J.* **76**, 300–306.

Conway, T. J. and Tans, P. 1990. *Atmospheric $CO_2$ concentrations*. The NOAA/GMCC Flask Sampling Network. CDIAC NDP-005/R1.

Di Pasquale, A. and Whitlock, C. H. 1993. First WCRP long-term satellite estimates of surface solar flux for the globe and selected regions. Proceedings of the ERIM/JOANNEUM RESEARCH/CIESN, *25th International Symposium on Remote sensing and global environmental change*. Graz, Austria, 4–8 April 1993.

Goward, S. N. and Dye, D. G. 1987. Evaluating North-American net primary productivity with satellite observations. *Adv. Space Res.* **7**, 165–174.

Hansen, J. and Lebedeff, S. 1987. Global trends of measured surface air temperature. *J. Geophys. Res.* **92**, 345–372.

Heimann, M. and Keeling, C. D. 1989. A three-dimensional model of atmospheric $CO_2$ transport based on observed winds (2). Model description and simulated tracer experiments. In: Aspects of climate variability in the Pacific and the Western Americas (ed. D. H. Peterson). *Geophysical Monograph* **55**, 237–274.

Heimann, M., Keeling, C. D. and Tucker, C. J. 1989. A three-dimensional model of atmospheric $CO_2$ transport based on winds (3). Seasonal cycle and synoptic time scale variations. In: Aspects of climate variability in the pacific and the western Americas (ed. D. H. Peterson). *Geophysical Monograph* **55**, 237–274.

Holben, B. N. 1986. Characteristics of maximum-value composite images from temporal AVHRR data, calibration. *Int. J. of Remote Sensing* **11**, 1511–1519.

Huete, A. R. 1989. Soil influences in remotely sensed vegetation-canopy spectra. In: G. Asrar (ed.): *Theory and applications of optical remote sensing*. John Wiley & Sons, New York, Chichester, Brisbane, Toronto, Singapore, pp. 107–140.

Janowiak, J. E. and Arkin, P. A. 1991. Rainfall variations in the tropics during 1986–1989, as estimated from observations of cloud-top temperature. *J. Geophys. Res.* **96** (suppl.), 3359–3373.

Kaufman, Y. J. and Holben, B. N. 1993. Calibration of the AVHRR visible and near-IR bands by atmospheric scattering, ocean glint and desert reflection. *Int J. Remote Sensing* **14**, 21–52.

Kergoat, L., Fischer, A., Moulin, S. and Dedieu, G. 1995. Satellite measurements as a constraint on estimates of vegetation carbon budget. *Tellus* **47B**, 000–000.

Kumar, M. and Monteith, J. L. 1981. Remote sensing of crop growth. In: *Plants and the daylight spectrum* (ed. H. Smith). London, New York, Toronto, Sydney, San Francisco: Academic Press, 133–144.

Leemans, R. and Cramer, W. P. 1991. *The IIASA database for mean monthly values of temperature, precipitation and cloudiness of a global terrestrial grid.* Research Report RR-91-18 November 1991, International Institute of Applied Systems Analyses, Laxenburg, Austria. 61 pp.

Lieth, H. 1975. Modelling the primary productivity of the world. In: *Primary productivity of the biosphere* (ed. H. Lieth and R. H. Whittaker). New York: Springer-Verlag, 237–263.

McCree, K. J. 1974. Equation for the rate of dark respiration of white clover as function of dry weight, photosynthesis rate and temperature. *Crop Science* **14**, 509–514.

McCree, K. J. 1972. Test of current definitions of photosynthetically active radiation against leaf photosynthesis data. *Agricultural Meteorology* **10**, 442–453.

Monteith, J. L. 1972. Solar radiation and productivity in tropical ecosystems. *J. of Applied Ecology* **9**, 744–766.

Monteith, J. L. 1977. Climate and the efficiency of crop production in Britain. *Philosophical Transactions of the Royal Society of London* **B281**, 277–294.

Olson, J. S., Watts, J. A. and Allison, L. J. 1983. *Carbon in live vegetation of major world ecosystems.* Environmental Science Division publication number 1997. Oak Ridge National Laboratory, Oak Ridge, Tennessee, USA.

Planton, S., Déqué, M. and Bellevaux, C. 1991. Validation of an annual cycle simulation with a T42-L20 GCM. *Clim. Dyn.* **5**, 189–200.

Ruimy, A., Dedieu, G. and Saugier, B. 1994. Methodology for the estimation of terrestrial net primary production from remotely sensed data. *J. Geophys. Res.* **99(D3)**, 5263–5283.

Sarmiento, J. L. 1993. Atmospheric $CO_2$ stalled. *Nature* **365**, 697–698.

Spangler, W. M. and Jenne, R. L. 1990. *World monthly surface station climatology.* Computer data tape documentation, National Center for Atmospheric Research, Boulder, CO, 74 p.

Stowe, L. L., Carey, R. M. and Pellegrino, P. P. 1991. Monitoring the Mt. Pinatubo aerosol layer with NOAA/11 AVHRR data. *Geophys. Res. Lett.* **19**, 159–162.

Tarpley, J. D., Schneider, S. R. and Money, R. L. 1984. Global vegetation indices from the NOAA-7 meteorological satellite. *J. Clim. Appl. Met.* **23**, 491–494.

Tucker, C. J., Fung, I. Y., Keeling, C. D. and Gammon, R. H. 1986. Relationships between atmospheric $CO_2$ variations and a satellite-derived vegetation index. *Nature* **319**, 195–199.

Whitlock, C. H., Charlock, W. F., Staylor, W. F., Pinker, R. T., Laszlo, I., DiPasquale, R. C. and Ritchey, N. A. 1993. WCRP surface radiation budget short-wave data product description, version 1.1. NASA Technical Memorandum 107747, NASA Langley Research Center, Compton, Virginia, USA.